BOREAS An international journal of Quaternary research

Chronology and palaeoenvironmental implications of the ice-wedge pseudomorphs and composite-wedge casts on the Magdalen Islands (eastern Canada)

AUDREY M. RÉMILLARD, BERNARD HÉTU, PASCAL BERNATCHEZ, JAN-PIETER BUYLAERT, ANDREW S. MURRAY, GUILLAUME ST-ONGE AND MARTIN GEACH

BOREAS

Rémillard, A. M., Hétu, B., Bernatchez, P., Buylaert, J.-P., Murray, A. S. , St-Onge, G. & Geach, M.: Chronology and palaeoenvironmental implications of the ice-wedge pseudomorphs and composite-wedge casts on the Magdalen Islands (eastern Canada). *Boreas.* 10.1111/bor.12125. ISSN 0300-9483.

The Magdalen Islands are a valuable terrestrial record, evidencing the complex glacial and periglacial history of the Gulf of St. Lawrence. Thirteen structures interpreted as ice-wedge pseudomorphs or composite-wedge casts were observed at four sites on the southern Magdalen Islands and testify to the former presence of permafrost under periglacial conditions. These features truncate Carboniferous sandstone or Last Glacial Maximum (LGM) glacial and glaciomarine diamicts, both overlain by subtidal or coastal units. Six optically stimulated luminescence (OSL) and four radiocarbon ages were obtained from both host and infilled sedimentary units. These ages provide the first absolute chronological data on these structures, shedding new light on the relationships between glacial and periglacial phases. Our chronostratigraphic data suggest that, after the deglaciation and the emersion of the archipelago, thermal contraction cracks grew during the cold period of the Younger Dryas (11–10 ka; 12.9–11.5 cal. ka BP). The Younger Dryas, which is well documented in the Maritime Provinces of Canada, occurred after a pedogenesis phase associated with the Allerød warm period evidenced by the well-developed palaeopodzol ubiquitous on the Magdalen Islands.

Audrey M. Rémillard (audrey.mercierremillard@uqar.ca) and Guillaume St-Onge, Institut des sciences de la mer de Rimouski (ISMER) & GEOTOP, Université du Québec à Rimouski, 310 allée des Ursulines, Rimouski, QC, G5L 3A1, Canada; Bernard Hétu and Pascal Bernatchez, Département de Biologie, chimie et géographie, Centre d'études nordiques (CEN), Université du Québec à Rimouski, 300 allée des Ursulines, Rimouski, QC, G5L 3A1 Canada; Jan-Pieter Buylaert and Andrew S. Murray, Nordic Laboratory for Luminescence Dating, Department of Geoscience, Aarhus University, Risø Campus, DK-4000 Roskilde, Denmark; Jan-Pieter Buylaert, Centre for Nuclear Technologies, Technical University of Denmark, Risø Campus, DK-4000 Roskilde, Denmark; Martin Geach, School of Geography, Earth and Environmental Sciences, Plymouth University, PL4 8AA Plymouth, UK; *received 11th September 2014, accepted 20th March 2015.*

The Magdalen Islands, located halfway between Prince Edward Island and Newfoundland in the Gulf of St. Lawrence (Fig. 1A), offer a strategic terrestrial record where the Last Glacial Maximum (LGM) glacial history in southeastern Canada can be investigated (e.g. Dredge *et al.* 1992). However, although extensive studies have focused on the palaeoenvironmental history of the islands, to date there is no consensus with regard to the glacial history of the archipelago (e.g. Richardson 1881; Chalmers 1895; Clarke 1911; Goldthwait 1915; Coleman 1919; Alcock 1941; Hamelin 1959; Prest *et al.* 1976; Dredge & Grant 1987; Parent & Dubois 1988; Dredge *et al.* 1992). Early research proposed that periglacial processes affected the archipelago during the LGM, but with no ice masses located on the islands themselves (Hamelin 1959; Poirier 1970; Laverdière & Guimond 1974; Dredge *et al.* 1992). This interpretation was based on a lack of recognizable glacial deposits across the islands and the high relative abundance of characteristic periglacial morphologies, such as ice-wedge pseudomorphs (Poirier 1970; Guilbault 1976; Dredge *et al.* 1992), cryopediments, and dry and asymmetrical valleys (Hamelin 1959; Laverdière & Guimond 1974; Paquet 1989). By contrast, recent regional models suggest that the maritime provinces of southeastern Canada were glaciated during the LGM, with the convergence of local icecaps, located on Nova Scotia, New Brunswick, Prince Edward Island and Newfoundland, with the Laurentide Ice Sheet (LIS) ice draining down the Laurentian Channel in the Gulf of St. Lawrence (Appalachian Glacier Complex; Stea *et al.* 1998, 2011; Josenhans & Lehman 1999; Stea 2004; Shaw *et al.* 2006; Josenhans 2007). Consistent with these models, Rémillard *et al.* (2013) described a subglacial diamict on the Havre-Aubert Island (Anse à la Cabane, Fig. 1B) from the Escuminac ice cap constrained between a periglacial colluvial deposit radiocarbon dated to *c.* 47–50 ka BP and frost-fissure infills dated to 13.2–12.2 cal. ka BP. These ages confirmed that the Magdalen Islands were glaciated at least during the Marine Isotopic Stage (MIS) 2 and suggested that periglacial conditions prevailed during MIS 3/early MIS 2, with the transition to glacial conditions during the LGM, and the onset of periglacial conditions once more after the LGM.

Recent developments in glacial modelling coupled with the increased precision of absolute dating methods highlight the spatial and temporal complexities in glacial dynamics in southeastern Canada. These complexities are still poorly described and our understanding is

DOI 10.1111/bor.12125

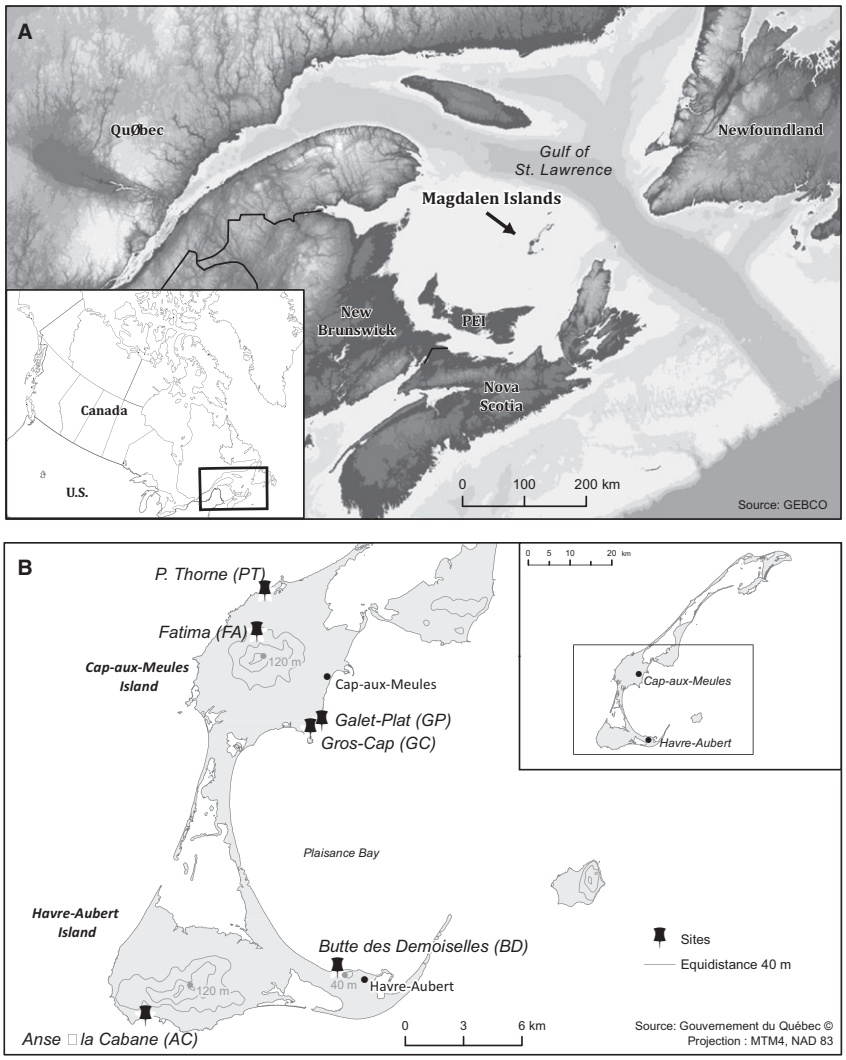

Fig. 1. A. Location of the Magdalen Islands in the Gulf of St. Lawrence and southeastern Canada. B. Locations of the Havre-Aubert and, Cap-aux-Meules Islands and sample sites on the Magdalen Islands.

limited by the extent and accessibility of key palaeoenvironmental records. The centralized location of the Magdalen Islands in the Gulf of St. Lawrence provides a very suitable site for the study of the terrestrial responses to glacial and periglacial dynamics both pre- and post-LGM are well preserved.

This study aimed to address hypotheses concerning the timing of periglacial activity and related climate conditions through the application of absolute dating methodologies within fissure structures located in the Magdalen Islands. Primary focus was placed upon the description of those frost-fissure wedges reported in Rémillard *et al.* (2013) supported by three new sites from the Havre-Aubert and Cap-aux-Meules Islands (Fig. 1B). Both radiocarbon dating and optically stimulated luminescence (OSL) dating were used to place the geomorphological data in a chronological context. OSL has been successfully applied before to relict sand wedges and composite pseudomorphs (e.g. Murton *et al.* 1997, 2000; French *et al.* 2003, 2007; Kovács *et al.* 2007; Buylaert *et al.* 2009; Liu & Lai 2013). In this study, we report on the chronology of the fissure structures located on the Magdalen Islands as well as their implication for the archipelago's glacial history. The new data are also discussed with reference to their palaeoenvironmental implications at the regional scale.

Geological and geomorphological setting

This study focused on samples derived from the Havre-Aubert and Cap-aux-Meules Islands (Fig. 1B). Both islands are composed of Carboniferous–Visean volcanic and sedimentary substrata (Brisebois 1981; Giles 2008). The geomorphology of the islands is dominated by basaltic conical hills surrounded by sandstone and shale platforms slightly inclined towards the sea, which

are interpreted as cryopediment surfaces (Laverdière & Guimond 1974; Paquet 1989). The sandstone is mainly composed of quartz contained in a calcareous and ferruginous cement; it is generally porous and friable, and so deeply weathered, to 1–2 m beneath ground surface (Brisebois 1981). On both islands, the bedrock is overlain by 0.5–6 m of Quaternary sediments (e.g. Dredge *et al.* 1992; Rémillard *et al.* 2013).

Methodology

Field observations

A total of four sites showing wedge structures was investigated in this study (Fig. 1B; Table 1). All site locations lie in areas of active coastal cliff retreat across the southern part of the archipelago. Two sites are located in the southern part of the Havre-Aubert Island: Butte des Demoiselles (BD) and Anse à la Cabane (AC), respectively located in the east and the west of the island (Fig. 1B). At each site, three structures were investigated. The remaining two sites are located on the Cap-aux-Meules Island, one in the northwest named P. Thorne (PT), and one in the southeastern part named Gros-Cap (GC). They contain three and four described structures, respectively. Two additional sites where involutions thought to be related to frozen ground are exposed were also studied: Fatima (FA) and Galet-Plat (GP) (Fig. 1B).

Particle size analysis

The grain-size distribution (<2000 μm) of both host and infill sediments of the wedge structures was determined with a Beckman–Coulter particle size analyser LS 13 320 (0.04– 2000 μm) on 41 disaggregated samples and processed with Gradistat software using the logarithmic method of Folk & Ward (1957) (Blott & Pye 2001).

Radiocarbon dating

Samples of organic material were collected from two structures in the AC site (AC-2; also presented in Rémillard *et al.* 2013) and from one fissure in the BD site (BD-1) for radiocarbon dating. The extracts were composed of undifferentiated plant detritus (no intact macrofossils such as leaves could be identified). Caution was taken to avoid the sampling of modern organic material (rootlets). The samples were prepared for radiocarbon dating at the radiochronology laboratory of Université Laval and analysed at the Keck Carbon Cycle AMS Facility at the University of California in Irvine. The conventional ^{14}C ages were calibrated using the CALIB 7.0 program with the INTCAL13 calibration data set (Reimer *et al.* 2013).

OSL dating

Samples for OSL dating were collected by hammering opaque plastic cylinders, 5 cm diameter and 30 cm long, into the most homogeneous central part of the structures' infills, at least 10 cm from the matrix. Samples were taken from the three fissures (OSL07, OSL14 and OSL15) and the host material (OSL06) at the AC site. A single sample was collected from the junction of the structures at the PT (OSL49) site and from host material at BD (OSL16). After sampling, it was visually checked that no host material had accidentally been included in the samples.

All OSL samples were prepared using standard sample preparation techniques. The outer ends of all tubes (~5 cm), potentially light-exposed during sampling, were used for water content measurements (natural and saturated) and dose rate analyses. All the unexposed parts of the samples were sieved to 180–250 μm and treated with 10% H_2O_2 (4 h), 10% HCl (2 h) to remove organics and carbonates, respectively (no visible reaction). Grains were subsequently etched in 10% HF for 20 min and heavy liquid separation (2.58 g mL^{-1}) was used to isolate a quartz-rich extract. This extract was etched for a further 1 h using concentrated HF (40%) to remove any remaining feldspar and to remove the outer alpha irradiated layer from the quartz grains.

Approximately 250 g of material was dried, ground and ashed (24 h at 450°C) and subsequently cast in wax in a fixed cup geometry. After 3 weeks of storage to let the ^{222}Rn reach equilibrium with its parent ^{226}Ra, the cups were counted on a high-resolution gamma spectrometer for at least 24 h following Murray *et al.* (1987). The radionuclide activities, water content, dry dose rates and total dose rates are given in Table 3.

Table 1. Location of sites and their elevation above sea level (a.s.l.), number of described structures for each site, ages and location of sampling for dating. N/A = not applicable.

Site	Latitude (N)	Longitude (W)	Elev. (m a.s.l.)	n structures	n ^{14}C ages	n OSL ages	Location of ^{14}C/OSL sample
BD	47.240490	61.865100	15	3	1	1	Infills and host material
AC	47.219500	61.995980	24	3	3	4	Infills and host material
PT	47.415120	61.910620	4	3	0	1	Infill
GC	47.351224	61.880630	5	4	0	0	N/A

All quartz OSL measurements were carried out with a Risø TL/OSL reader (model DA-20) equipped with blue LEDs (~80 mW cm^{-2}) and IR LEDs (~135 mW cm^{-2}) (Thomsen *et al.* 2006). Large (~8 mm) aliquots were prepared on stainless steel discs using Silkospray as a fixating agent. During preliminary measurements, weak infrared stimulated luminescence (IRSL) signals (<7% of blue light stimulated luminescence) were observed but the purity of the quartz extracts was confirmed by an OSL IR depletion test (Duller 2003); all samples had OSL IR depletion ratios within 10% of unity.

The single-aliquot regenerative-dose (SAR) procedure was used for equivalent dose (D_e) determination (Murray & Wintle 2000, 2003). Quartz aliquots were stimulated using blue light at 125°C for 40 s. The D_e values were calculated using early background subtraction (signal: 0.00–0.32 s, background: 0.32–0.64 s) (Cunningham & Wallinga 2010). Figure 2A illustrates a representative dose response curve and natural decay curve (inset) for sample OSL15. The quartz OSL decay curve is clearly dominated by a fast component (compare to the decay curve of calibration quartz; Hansen *et al.* 2015) making it suitable for quartz OSL dose determination using SAR (Wintle & Murray 2006). A thermal transfer test was carried out using sample OSL14; 24 aliquots were exposed to blue light at room temperature for 100 s, stored for 10 ks and exposed again to blue light. The residual doses were then measured in the usual manner (Fig. 2B). From this curve, we adopted a preheat ≤200°C (cut-heat 40°C lower than preheat) for all D_e determinations. A dose recovery test was then undertaken on all samples using two 40-s periods of blue LEDs bleaching at room temperature (separated by 10 ks pause) followed by a beta dose approximately equal to the natural. This dose was then measured in the usual manner using a preheat of 200°C (cut-heat 160°C) and the mean dose recovery ratio was 0.95±0.02 (n=36). This result suggests that our chosen SAR protocol is suitable for these samples.

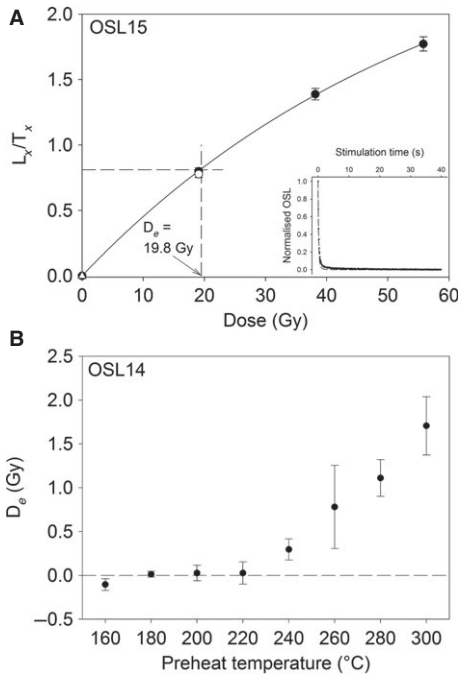

Fig. 2. A. SAR dose response curve from sample OSL15 (AC-3 structure). Regenerated signals are shown as filled circles. The unfilled circle represents a recycled point and the unfilled triangle a zero Gy dose point (recuperation). Inset shows typical natural OSL decay curve from the same sample together with a decay curve of an aliquot of calibration quartz (dashed). B. Thermal transfer plateau for sample OSL14 (AC-2 structure); error bars represent one standard error.

Results

Butte des Demoiselles (BD)

The BD exposure is a ~15-m-high active coastal cliff. Three sedimentary units lie on red mudstone substrata (Fig. 3). Unit 1 (U1) is a 1–5 m thick diamict composed of silty fine sand (Table 2), which has been interpreted as being deposited in a glaciomarine environment during the last deglaciation (cf. Rémillard *et al.* 2013: p. 560). A subtidal stratified fine sand unit (U2; Table 2) 50–150 cm thick overlies U1. This unit was sampled for OSL dating (OSL16) and the resulting age is 11.1±0.8 ka (Table 3; Fig. 3A). The uppermost unit (U3) is a 30–50 cm thick eolian deposit that covers a fossil soil characterized by a light grey horizon of eluvial origin which is actually the Ae horizon of a palaeopodzol ubiquitous on the Magdalen Islands. Three structures were observed at two sites located at ~400 m from each other. The top of these structures is located between 40 and 70 cm depth beneath the ground surface.

The most eastern location has two structures, BD-1 and BD-2 (Fig. 3A, B). BD-1 starts ~40 cm depth beneath the ground surface and goes down to a depth of 165 cm, i.e. up to the contact with U1. It is 60 cm wide at the top, ~30–35 cm halfway down, and a few cm at the tip (Fig. 3A). The fissure consists of two zones: a narrow, structureless inner zone derived from the layers above (iA) and from the sides (iB), and an outer zone of host sediments affected by normal microfaults (nf) to at least 15–30 cm on each side of the inner zone. The downward bending of U2 beds (dtb) can also be seen on both sides of the structure.

BD-2 is located ~20 m from BD-1. With a height of 90 cm, BD-2 starts ~60 cm beneath the ground surface, fully penetrates U2, and then enters ~45 cm into the top of U1; the apex is located at ~150 cm beneath the ground surface (Fig. 3B). This structure can be divided into two parts, adjacent to the contact between U1 and U2. The bottom part is 50 cm thick and 30 cm

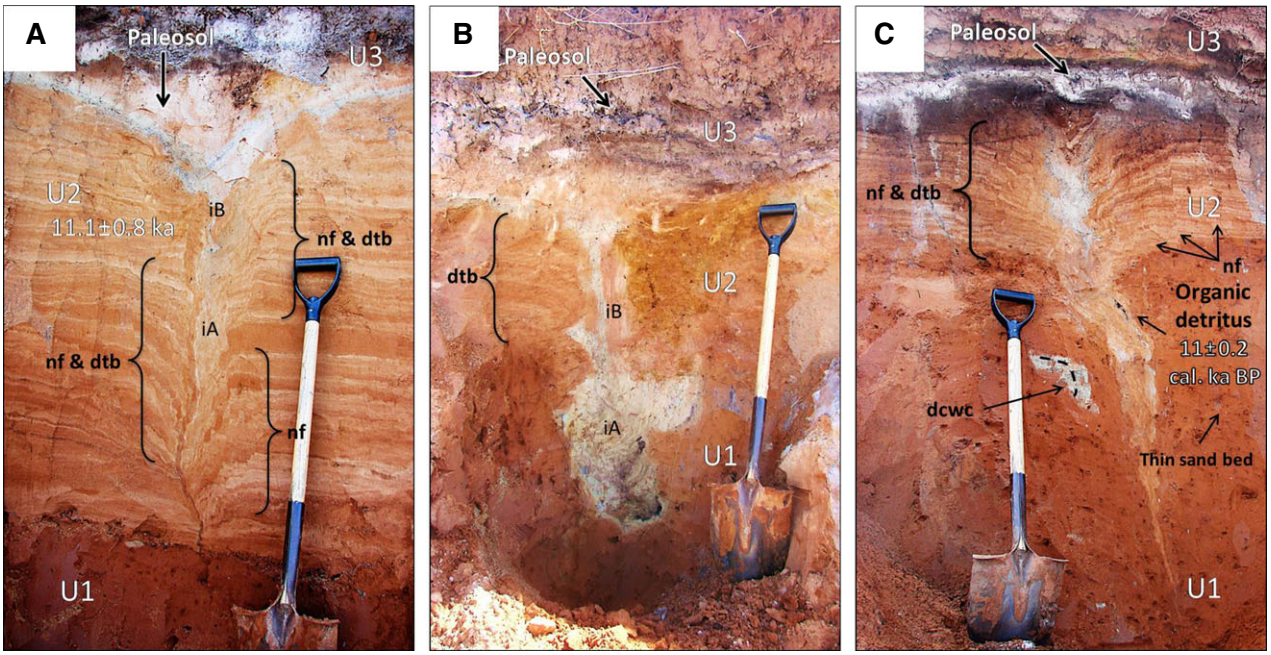

Fig. 3. Buttes des Demoiselles (BD) structures. U1 = sandy glaciomarine diamict; U2 = subtidal stratified sand; U3 = eolian sand; nf = normal fault; dtb = downturned beds; dcwc = down-curved weathered clast. iA and iB correspond to the different infillings (see text). A. BD-1. B. BD-2. C. BD-3. Note: OSL16 was collected in U2 of BD-1 (not shown in the pictures).

Table 2. Particle size data from the study. N/A = not applicable.

Site	BD enclosing sediment		BD infills			AC enclosing sediment		AC infills			GC enclosing sediment		GC infills
Unit	U1	U2	BD-1	BD-2	BD-3	U1	U2	AC-1	AC-2	AC-3	U1	U2	N/A[1]
Description	Glaciomarine	Subtidal				Glacial	Subtidal				Sandstone	Coastal	
n	3	3	1	1	1	5	7	3	3	4	2	2	6
Medium to coarse sand (%)	0.5	1	1	0	1	5	3	0	0	0	1	56	29
Fine to very fine sand (%)	71.5	84	77	85	86	54	77	77	77	75.5	89	32	58
Silt (%)	25	13	20	14	12	33	18	21	21	23.5	9	10	11
Clay (%)	3	2	2	1	1	8	2	2	2	2	1	2	2
Mean size (μm)	75	110	81	105	112	45	90	82	81	77	116	283	184
Mean size (ϕ)	3.87	3.19	3.63	3.25	3.16	4	3.5	3.62	3.65	3.72	3.1	1.9	2.5
Sorting (ϕ)	1.49	1.12	1.36	0.91	0.98	2.2	1.2	1.00	1.10	1.16	0.54	1.76	1.54
Skewness (ϕ)	0.57	0.39	0.58	0.38	0.32	0.50	0.46	0.43	0.42	0.50	0.20	0.26	0.01
Kurtosis (ϕ)	1.83	2.30	2.07	1.67	1.99	1.15	2.08	2.12	1.92	2.03	1.13	1.82	1.44

[1]Average of the matrix (<2000 μm) of six different infills at the GC site.

wide and is composed essentially of white sand and disintegrated organic matter (iA). It is characterized by an irregular morphology marked by a widening (right side) at ~30 cm height from the tip. The top part is 40 cm thick and only 15 cm wide. The infilling material of the top part can be divided into two different zones: the centre is filled with white sand coming from the palaeosol whereas the edges are filled by reddish sand from unit U2. On the left side of the structure, U2 beds are bent downward ('dtb' on Fig. 3B). Vertical laminated structures (iB) are also present at the centre of the wedge.

BD-3 occurs 50 cm beneath the ground surface, under a 15-cm-thick fossil soil. This structure fully penetrates U2, and enters 50 cm into U1 (Fig. 3C) to give a total height of 170 cm. The structure is 60 cm

Table 3. Sample location, depth, radionuclide concentrations, water content, total dose rates, equivalent doses (D_e) and resulting luminescence ages. Radionuclide concentrations were converted to dry infinite matrix dose rates using the conversion factors of Guérin *et al.* (2011).

Site	Sample ID	Structure	Depth (cm)	Radionuclide activities (Bq kg^{-1})				Dry dose rate (Gy ka^{-1})		Water content measurements (%)			Total dose rate (Gy ka^{-1})	D_e (Gy)	n	OD (%)	Age (ka) (±1σ)
				^{238}U	^{226}Ra	^{232}Th	^{40}K	Gamma	Beta	Nat.	Sat.	Life time avg.					
AC	OSL14	AC-1	50	45±4	24.8±0.4	23.5±0.3	539±8	0.87±0.02	1.72±0.03	9	42	21	2.24±0.12	22.6±1.0	24	16	10.1±0.7
AC	OSL07	AC-2	110	39±7	23.5±0.6	21.1±0.6	557±12	0.86±0.02	1.72±0.04	8	34	17	2.28±0.13	22.4±0.8	21	14	9.8±0.7
AC	OSL15	AC-3	100	29±7	21.6±0.6	16.9±0.6	512±12	0.75±0.02	1.54±0.04	8	33	17	2.06±0.12	22.1±0.5	27	11	10.7±0.7
AC	OSL06	Host material	75	26±5	20.9±0.4	20.5±0.5	489±10	0.78±0.02	1.49±0.03	10	40	20	1.99±0.11	23.1±0.5	27	10	11.6±0.7
BD	OSL16	Host material	150	26±5	14.7±0.4	14.2±0.4	474±10	0.65±0.02	1.39±0.03	12	42	21	1.76±0.09	19.6±0.9	21	21	11.1±0.8
PT	OSL49	Junction	15	42±4	14.3±0.3	18.3±0.3	503±8	0.71±0.01	1.54±0.03	12	32	16	2.10±0.11	26.9±1.1	39	22	12.8±0.9

wide at the top including host material deformations and quickly tapers downwards in the diamict where it ends in a narrow tip. The infilling is divided into two zones. At the bottom (U1 level), the first zone is composed of fine to medium sand that bears sedimentological similarities with the subtidal overlying unit (U2), but showing some sub-vertical lamination. Some sub-vertical lenses of light grey sand that seem to belong to the overlying Ae horizon can also be found in this zone. Halfway up the structure, a vertical lens of organic matter (1 cm wide, 8 cm height) seems to come from the palaeosol. This lens was dated by radiocarbon to 11.0±0.2 cal ka BP (UCIAMS-121093; Fig. 3C; Table 4). On either side of BD-3, U1 shows sagging; a thin sand bed and a weathered argillite pebble downwarp towards the fissure tip (Fig. 3C). The top of U1 is also bent downward on either side of the structure. The second infilling zone is located at the U2 level. The central part is characterized by light grey sand similar to the Ae horizon. The interlayered nature of this whitish infilling suggests infiltration of this material while the host material was downwarping. On either side of the grey sand, the infill corresponds to U2. The host sediment is characterized by normal and *en echelon* microfaults to at least 30 cm on each side of the structure.

Anse à la Cabane (AC)

The exposure is located in the western part of Anse à la Cabane, to the south of the Havre-Aubert Island (Fig. 1B). Three fissures are located at ~10–15 m from each other at an elevation of ~24 m a.s.l. They penetrate the two different units that lie on the bedrock (Fig. 4). The first (lower) unit (U1) is a MIS 2 silty-sand glacial diamict more than 3 m thick (cf. Rémillard *et al.* 2013: p. 559). The second unit (U2) is composed of interbedded red and white fine sand (Table 2) about 100 cm thick and interpreted as a subtidal unit deposited during the postglacial marine transgression. The top of the latter unit has been ploughed to a depth of 30 cm, which removed the palaeopodzol (some lenses remain). The subtidal unit (U2) was sampled for OSL dating (OSL06) next to the AC-2 structure (Fig. 4B), and gave an age of 11.6±0.7 ka, consistent with the OSL age (11.1±0.8 ka) obtained for the subtidal unit (U2) at the BD site.

Table 4. List of radiocarbon ages presented in this paper. Note that AC samples were also presented in Rémillard *et al.* (2013).

Site	Structure	Laboratory ID	Age ^{14}C a BP±1σ	Calibrated age±1σ
BD	BD-3	UCIAMS-121093	9650±35	10 991±198
AC	AC-2	UCIAMS-84795	11 230±30	13 122±158
AC	AC-2	UCIAMS-84790	10 935±30	12 793±136
AC	AC-2	UCIAMS-74415	10 485±25	12 405±170

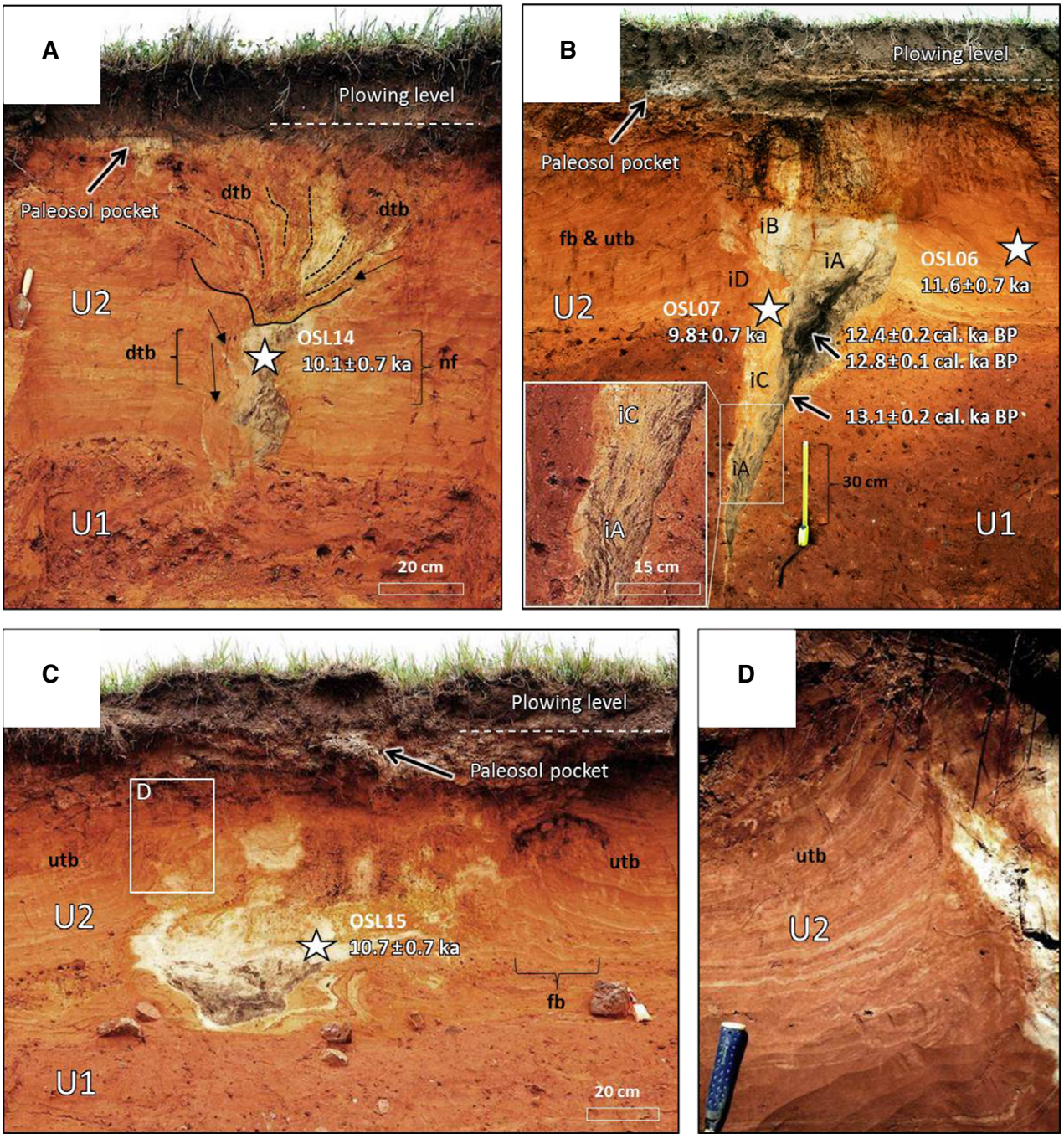

Fig. 4. Anse à la Cabane (AC) structures. Stars correspond to OSL sample locations. U1 = glacial sandy diamict; U2 = subtidal stratified sand; nf = normal fault; dtb = downturned beds; utb = upturned beds; fb = folded beds. A. AC-1. B. AC-2. iA, iB, iC and iD correspond to the different infillings (see text). C. and D. AC-3.

The structure AC-1 is 130 cm high beneath 30 cm of soil. It penetrates and deforms mainly U2 (and penetrates only ~20 cm into U1; Fig. 4A). This is a relatively complex structure, which can be divided into two parts. In the lower half, the structure is 25–35 cm wide. The infill material is divided into three parts. To the bottom right, there is grey sand mixed with organic matter. The grey silty-sand (Table 2) was sampled for OSL dating (OSL14) and gave an age of 10.1±0.7 ka (Fig. 4A; Table 3). There is also a thin strip of grey sand that lines the bottom and left wall of the structure. The remaining infill is composed of a block of undulated beds of U2, which seems to have sagged downwards into the structure. The host material is deformed; to the right, there are several normal *en echelon* microfaults whereas to the left, beds of U2 dip

downward. The infilling sediments seem to have been truncated in the central part of the structure, probably by gullying. The upper half of the infilling is partly composed of sand that probably belongs to U2. The sub-stratification orientation (like an overturned fold) suggests that U2 slipped into a central depression. According to the bending of the beds, it is obvious that most of the sediments come from the left side and were ductile.

AC-2 starts 60 cm beneath the ground surface and has a height of 150 cm. It crosses both the U1 and U2 units (Fig. 4B). The structure is characterized by a very well-defined V-shaped morphology; at the top, the cast is 80 cm wide whereas it is only a few millimetres at the apex. The beds in the subtidal host material show an upward bending and folding. The infilling material is divided into four parts, iA to iD. The first one (iA) is composed of white sand mixed with organic matter. Vertical stratifications characterize the bottom part of the fissure showing an alternation of white organic sand and reddish sand (Fig. 4B, inset). The second part (iB) of the infilling is composed of vertically laminated white sand, which forms an outgrowth above the main part of the structure. The iC and iD infilling are characterized by red and white silty-sand similar to U2 (Table 2); iC is rather structureless and iD has preserved U2 stratification but seems to have slipped downward. A sample (OSL07) was collected in iC for OSL dating. The resulting age is 9.8±0.7 ka. Three samples of organic matter were collected for radiocarbon dating: one at 40 and two at 90 cm from the fissure apex (Fig. 4B). These samples gave ages of

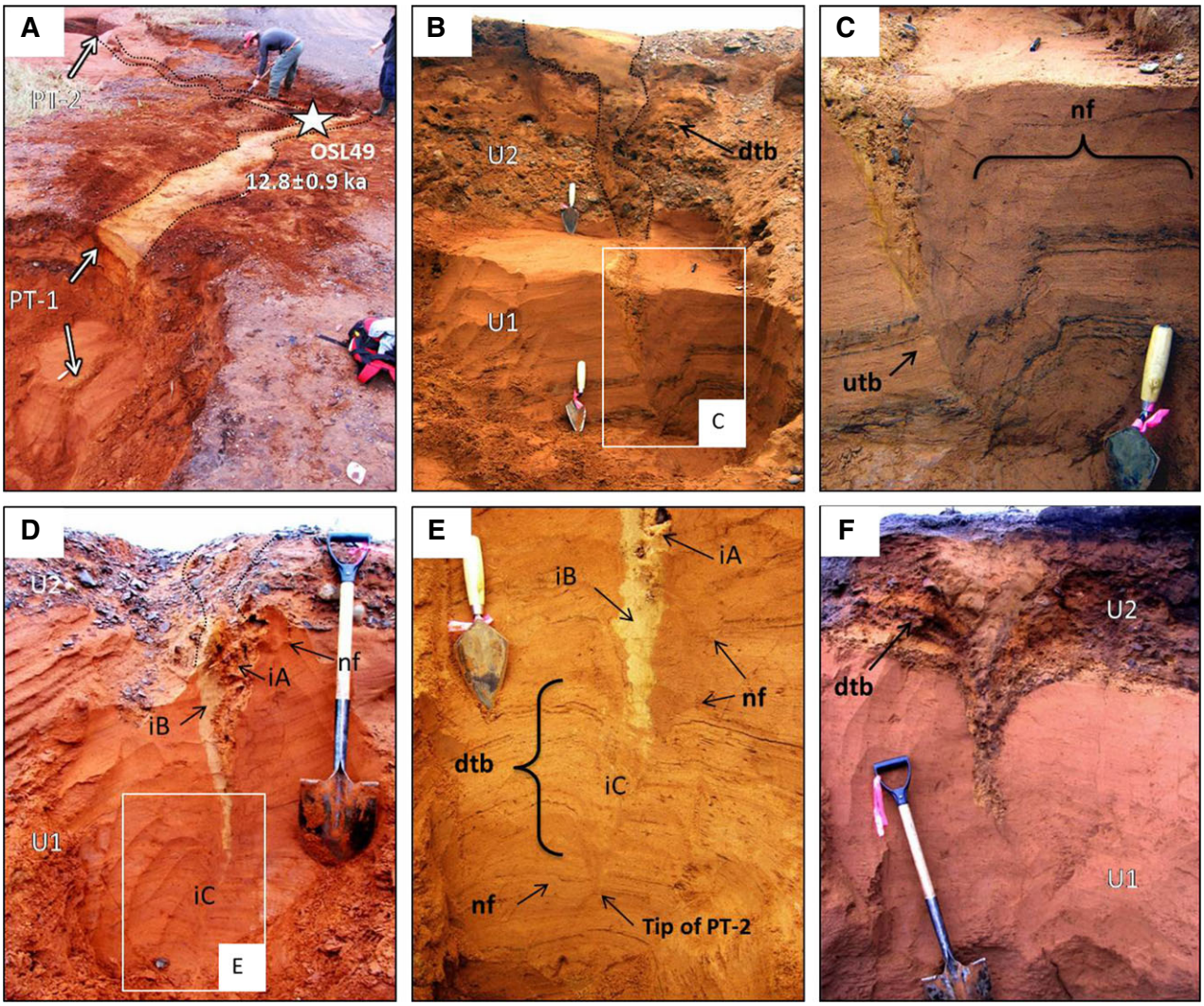

Fig. 5. P. Thorne (PT) structures. U1 = weathered Carboniferous sandstone; U2 = coastal sand and gravel; nf = normal fault; utb = upturned beds; dtb = downturned beds. A. Junction of structures' network (star corresponds to OSL sample location). B. PT-1. C. Close-up of the bottom part of PT-1. D. PT-2, iA, iB and iC correspond to the different infillings (see text). E. Close-up of the bottom part of PT-2. F. PT-3.

13.1±0.2 cal. ka BP (UCIAMS-84795) at 40 cm, and 12.8±0.1 cal. ka BP (UCIAMS-84790) and 12.4±0.2 cal. ka BP at 90 cm (Table 4).

AC-3 is 130 cm high and more than 100 cm wide (Fig. 4C). It occurs beneath a ~50-cm-thick soil. The structure truncates and deforms only U2, and is characterized by a bowl-shaped morphology. To the right bottom part, U2 is deformed by folds. U2 is deformed by folds in the right bottom part. On either side of the structure, U2 beds curve upwards and produce lateral thrust (Fig. 4D). The infill of AC-3 is divided into two different zones, the apex and the top. The apex is ~50 cm thick and is composed essentially of disintegrated organic matter and white silty-sand (Table 2). The latter was sampled for OSL dating (OSL15) and gave an age of 10.7±0.7 ka (Fig. 4C; Table 3). The top part is ~75 cm thick and is composed of structureless white and reddish sand and light grey sand pockets.

P. Thorne (PT)

The three structures found at PT penetrate the weathered sandstone platform (U1) and the overlying 50–100 cm thick unit of coastal stratified sand, gravel and pebbles (U2) (Fig. 5). The top of the cliff is 4 m a.s.l. Owing to municipal works conducted at this site, the uppermost part of the section (~50 cm) has been removed, exposing the network connecting the structures (Fig. 5A). A sample of the fine sediment infill was collected for OSL dating (OSL49) at the network junction; this gave an age of 12.8±0.9 ka for the wedge infill (Table 3).

PT-1 is 170 cm high and penetrates through U2 and into U1 (Fig. 5A–C). The width of the structure is 40 cm at the top and quickly decreases to 15 cm and then gradually narrows to the apex. The infilling is divided into three zones. The first zone is the rectangular shape at the top of the structure and is composed of well-sorted, light brown sand (Fig. 5A, B). Comparison of this sand with the host material suggests that it probably has another origin. The second zone is located between 20 and 150 cm depth and is composed of coarse sand and pebbles similar to U2. The pebbles are mostly vertically orientated. Between 150 and 170 cm depth, the infilling corresponds to faulted weathered sandstone, as illustrated by normal microfaults and downward curved beds on the right bottom part (Fig. 5B, C). Host strata are also deformed downwards in the upper part of the structure (U2; Fig. 5B) and slightly upturned on the left bottom part (Fig. 5C).

PT-2 is 40 cm wide near the surface (Fig. 5D). It tapers into U2 to a depth of 140 cm. The infilling comprises three zones: iA on the right side is composed of sand and pebbles sagged to a depth of 80 cm (U2); iB is to the left side and comprises light brown sand up to 110 cm depth; and iC is the apex zone of the structure between 110 and 140 cm depth and is filled by weathered sandstone (U1). The lower part of the host material is characterized by downturned strata (left) and normal microfaults (right) (Fig. 5E). Microfaults occur also in the host sediment to the upper left side of the structure.

PT-3 shows a well-defined V-shaped morphology and is more than 150 cm high (Fig. 5F). It crosses U2 and enters U1 at a depth of 65 cm. The lower part of the host material (U1) is too homogeneous to allow the observation of any deformation. However, it is obvious that the shoulders of the weathered sandstone have sagged on either side of the structure. In the upper part, both sides of the structure show downturned host strata (U2). The infill is mostly characterized by sand and pebbles from U2 that fell into the depression. The upper part of PT-3 is filled by light brown sand, similar to the upper infilling of PT-1 and PT-2.

Gros Cap (GC)

Ten fissures were observed on the northern cliff of the GC site (Fig. 1B). They are 130–170 cm high and spaced between 2.5 and 12 m from each other. They truncate the sandstone platform (U1) and a stratified 50–100 cm thick sand and pebbles coastal unit (U2) (Fig. 6). As they are quite similar, only four are presented here. They occur in the lower part of U2 and penetrate U1 at a depth of 100–120 cm. The top of the fissures are located between 30 and 60 cm beneath the ground surface. All structures show a well-defined V-shaped morphology. Host strata are deformed upwards. The infillings are composed of coarse sediment from U2; the sediment becomes finer-grained from top to bottom and the pebbles are vertically aligned.

Involutions

Involution structures were observed at two different sites on the Cap-aux-Meules Island (Fig. 1B): Galet-Plat (GP) and Fatima (FA) (Fig. 7). The GP site is located on the southeastern part of the island and corresponds to an active coastal cliff ~5 m high (Fig. 7A, B). The FA site is a trench, several tens of metres long, dug for road construction on the western part of the Cap-aux-Meules Island (Fig. 7C, D). At both sites, vertical sections expose two units. Unit 1 (U1) corresponds to the highly weathered sandstone platform and Unit 2 (U2) to a ~0.75-m-thick coastal deposit composed of pebbles lying in a poorly sorted sand matrix. The interface between the two units displays tapered upward-extending injections and round bulges and downward-extending lobes (not tapered). The amplitude of these involutions varies between ~0.5 and 0.75 m (Fig. 7).

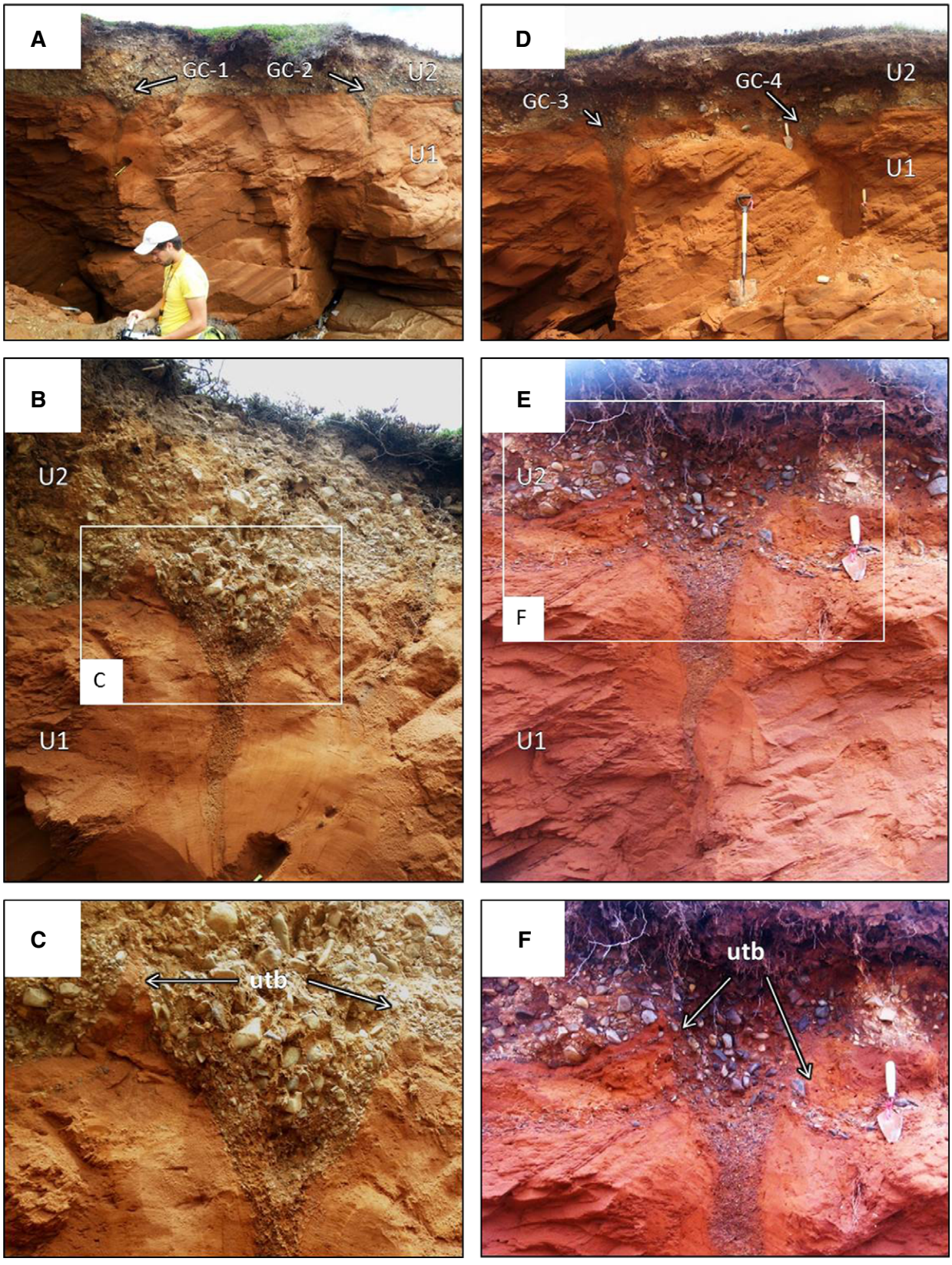

Fig. 6. Gros-Cap (GC) structures. U1 = Carboniferous sandstone; U2 = coastal sand and gravel; utb = upturned beds. A. GC-1 and GC-2 locations. B. GC-1. C. Close-up of GC-1 shoulders. D. GC-3 and GC-4 locations. E. and F. GC-3. Note that the sediment gets finer-grained from top to bottom and that the pebbles are vertically aligned in all structures.

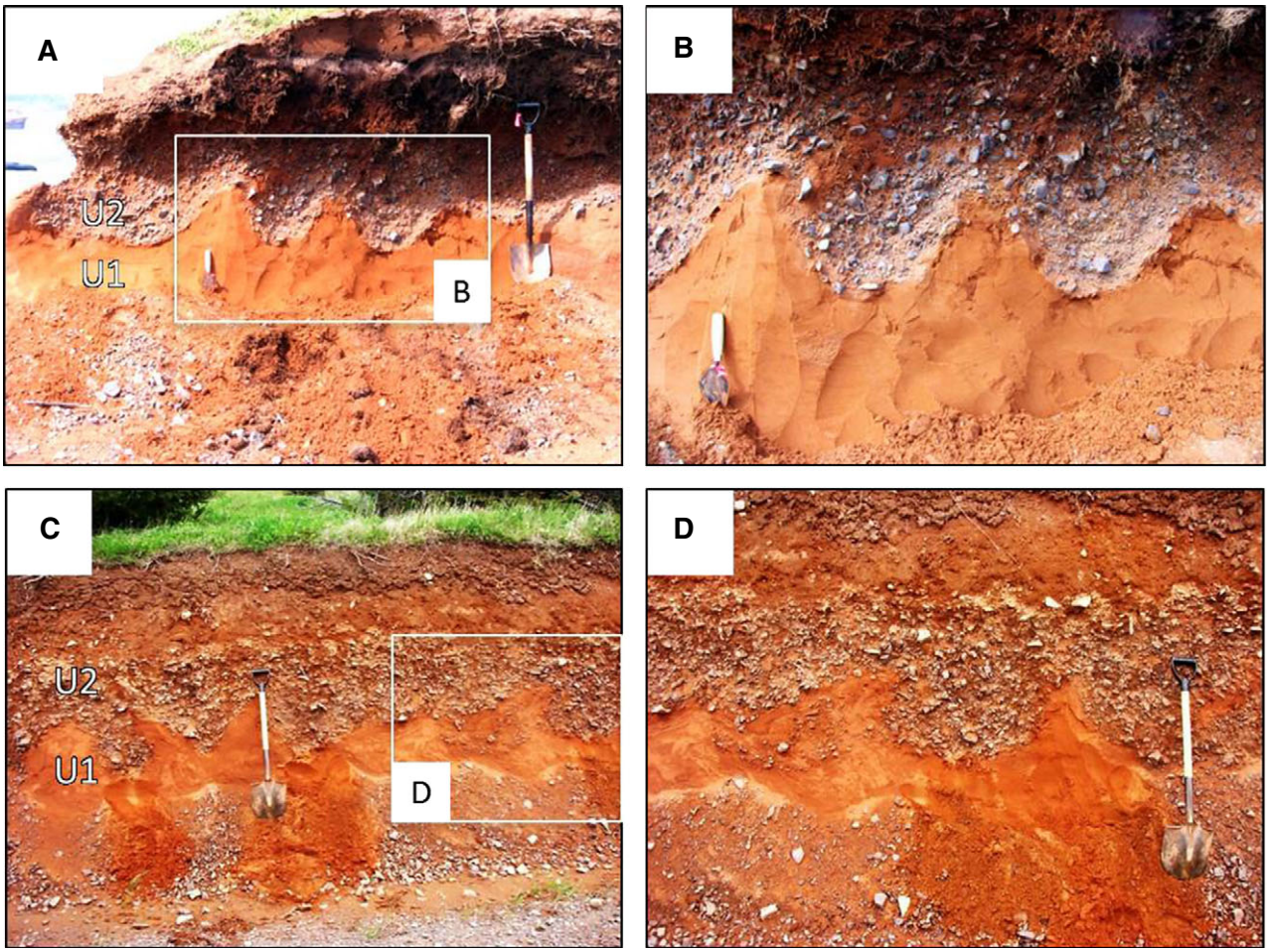

Fig. 7. Involutions interpreted as cryoturbations on the Cap-aux-Meules Island. U1 = highly weathered sandstone bedrock; U2 = coastal deposit composed of pebbles with poorly sorted sand matrix. A. Involutions at the GP site. B. Close-up of the involutions at the GP site. C. Involutions at the FA site. D. Close-up of the involutions at the FA site.

Discussion

Origin of the structures

We interpret the structures described above as frost-fissure wedges resulting from thermal-contraction cracking formed in permafrost. Frost-fissure wedges can be confused with other features that have no connection with permafrost effects. The most common are seismic structures, desiccation cracking, water-escape structures and clastic dikes (Black 1976; French 2007). Water-escape features are generally connected to an underground drainage network or a more permeable layer and the resulting structures are vertical, oblique or even horizontal; these cylindrical (pipes) structures are often filled with circular layers (Gangloff 1974; Cheel & Rust 1986; Johnson 1986; Dionne & Pérez Alberti 2000; Dionne & Laliberté 2005). In Quaternary sediments, clastic dikes often have a seismic or a glaciotectonic origin. These features can be of different forms compared with frost-fissure wedges (e.g. reversed wedge, irregular branched form), and are often intraformational. Generally, clastic dikes cut across the enclosing beds suddenly without deforming the host material. These features are often found with other structures such as (i) low-angle thrust-faulted rafts, brecciated melange in a shear zone between thrust-faulted rafts, different types of folds (glaciotectonic origin) (Rémillard *et al.* 2013; Ravier *et al.* 2014; Vaughan *et al.* 2014), and (ii) ball-and-pillow, plastic intrusion, disturbed lamination, convolute stratification and slumps, sand dykes, autoclastic breccias and sand volcanoes (seismic origin) (Berra & Felletti 2011; Brandes & Winsemann 2013; Su *et al.* 2014). None of these different structures has been found in the host material of the frost-fissure wedges on the Magdalen Islands, and in any case, the archipelago is not located in a seismic zone. Generally, desiccation cracks are much smaller than the fissures described on the archipelago (Li & Zhang 2011). Giant desiccation cracks and polygons do occur in playas but they form in fine sediment (2 μm grain size on average) and not

Fig. 8. The asymmetrical valley eroded into the sedimentary succession of the AC site. View toward south.

in sand or gravel (Neal *et al.* 1968; El Maarry *et al.* 2012). Based on the characteristics described above, all these different potential origins can be reasonably eliminated for the structures observed on the Magdalen Islands.

Another parameter that should be considered when discussing whether or not the structures result from thermal-contraction cracking is the suitability of the host material for such cracking. Thermal cracking occurs when the tensile stress produced by thermal contraction exceeds the tensile strength of the soil and generates this cracking (Fortier & Allard 2004). The coefficient of thermal expansion expresses the relative capability of the material to be 'moved' when subject to the tensile stress produced by thermal contraction. The coefficients of thermal expansion vary depending upon numerous parameters (temperature, rate of cooling, duration of cold spells, granulometric composition, unfrozen water content, etc.), but in general, the coefficients tend to increase from sand to finer sediment (silty-clay) and with water (ice) content (e.g. Mordovskii *et al.* 1993; Mackay & Burn 2002). In palaeoenvironmental reconstructions, it is possible to examine only a few factors when analysing the probable coefficient of thermal expansion, such as the particle size and the most likely water content at the time of wedge development. Particle-size analysis data indicate that U1 and U2 at both the BD and AC sites have a mean grain size between 45 and 75 μm and 90 and 100 μm, respectively (Table 2). At the PT and GC sites, each structure penetrates significantly into the sandstone bedrock. Particle size analysis carried out on this bedrock gave a mean size of 116 μm; almost 90% of the sandstone is composed of fine to very fine sand, and 10% of silt and clay. These data indicate a matrix more favourable to contraction cracking than in coarser sand or gravelly deposits. In addition, the wedges formed in the Magdalen Islands developed in subtidal (BD and AC sites) and coastal (PT and GC sites) sediments. The water content of these sediments was undoubtedly high (probably at saturation or close to saturation) when they began to freeze, favouring thermal-contraction cracking.

The well-developed periglacial landscape on the Magdalen Islands also suggests that the structures probably have a cryogenic origin. The most ubiquitous periglacial features are cryopediments and dry and asymmetrical valleys (Laverdière & Guimond 1974; Paquet 1989). It is important to note that there is no river or perennial creek on the Magdalen Islands owing to the high porosity of the sandstone bedrock, which favours infiltration. The cryopediments and asymmetrical valleys needed the presence of perennially frozen ground to block the infiltration of water that lead to the runoff (surface flow) forming these slightly inclined morphologies (Laverdière & Guimond 1974; Paquet 1989). At the AC site, an asymmetrical valley was eroded into the sediments in which the frost-fissure wedges were formed (U1, U2 and the underlying bedrock; Fig. 8). The age of this valley is therefore $<11.6\pm0.7$ ka (age of the host sediment U2) and is maybe contemporary with the frost-fissure wedges of the AC site. The formation of this valley after the emergence of U2 at this site indicates that the structures were formed in a permafrost environment characterized by active periglacial processes.

There is also a cryostratigraphical argument to consider when discussing the origin of the structures. The frost-fissure wedges observed on the Magdalen Islands are located between 30 and 70 cm beneath ground surface. The sediment layer above the structures is interpreted as the palaeo-active layer. This

Table 5. Field observations and measurements of the ice-wedge pseudomorphs described in this paper. N/A = not applicable.

Site	Structure ID	Maximum depth (cm)	Maximum width (cm)	Contacts	Infill (OD = organic detritus)	Morphology	Upturned host strata	Downturned host strata	Realigned pebbles	Other features
BD	BD-1	125	60	Notsharp, deformed	Sand	V-shaped		✓	N/A	Normal microfaults in host sediment
	BD-2	90	40	Notsharp, deformed	Sand and OD	Bowl-shaped		✓	N/A	Vertical laminated structures
	BD-3	170	60	Sharp, deformed	Sand and OD	V-shaped		✓	N/A	Gravitational microfaults
AC	AC-1	130	80	Notsharp, deformed	Sand and OD	V-shaped		✓	N/A	Several normal microfaults
	AC-2	150	80	Sharp, undeformed	Sand and OD	V-shaped	✓		N/A	Vertical laminations
	AC-3	130	100	Sharp, deformed	Sand and OD	Bowl-shaped	✓		N/A	Folds in host sediment
PT	PT-1	170	40	Sharp, undeformed	Sand and pebbles	V-shaped		✓	✓	Normal microfaults in host sediment
	PT-2	140	40	Sharp, undeformed	Sand and pebbles	V-shaped		✓	✓	Normal microfaults in host sediment
	PT-3	150	60	Sharp, undeformed	Sand and pebbles	V-shaped		✓	✓	Inverse grading of infilling sediment
GC	GC-1	140	50	Sharp, undeformed	Sand and pebbles	V-shaped	✓		✓	Inverse grading of infilling sediment
	GC-2	130	40	Sharp, undeformed	Sand and pebbles	V-shaped	✓		✓	Inverse grading of infilling sediment
	GC-3	170	60	Sharp, undeformed	Sand and pebbles	V-shaped	✓		✓	Inverse grading of infilling sediment
	GC-4	150	40	Sharp, undeformed	Sand and pebbles	V-shaped	✓		✓	Inverse grading of infilling sediment

interpretation is supported by the involutions observed in some places on the islands (e.g. Fig. 7), firmly identified as cryoturbations. Cryoturbations have been recognized as an indicator of past permafrost occurrence or deep seasonal frost: <0.6 m amplitude cryoturbations are related to deep seasonally frozen ground, whereas those of ≥0.6 m amplitude are more likely to occur in continuous permafrost environments (e.g. Murton & French 1993; Huijzer & Isarin 1997; Van Huissteden *et al.* 2003; Vandenberghe *et al.* 2004; Ogino & Matsuoka 2007; French 2008; Bertran *et al.* 2014; Fábián *et al.* 2014). On the Cap-aux-Meules Island, the amplitudes of the cryoturbations are ~0.5 and 0.75 m. As their amplitudes are at the limit of what is considered in the literature as being an undoubtedly permafrost-related feature, their amplitude alone cannot be used as a conclusive argument for permafrost conditions. However, under current drainage conditions, the substratum is too dry to allow the formation of such features. To allow water saturation of the active layer, the sandstone bedrock must have been frozen (impermeable) under the thin sediment layer (Fig. 7). Thus, the cryoturbations also point to the former presence of permafrost. Furthermore, both the top of the frost-fissure wedges and the bottom of the cryoturbations occur at ~0.7 to 1 m depth. This could suggest that they are likely to have been formed during the same periglacial event.

Nature and evolution of the frost-fissure wedges

Based on the arguments discussed above, it appears that the structures observed on the Magdalen Islands resulted from thermal-contraction cracking in permafrost conditions, under an active layer ~1 m thick. In current permafrost environments, a variety of frost-fissure wedges occurs depending on the type of infill. Frost-fissure wedges with a primary infill of sediment are referred to as 'sand-wedges' whereas the fissures with an initial infill of ice are referred to as 'ice-wedges'. The relict forms of these two types of wedges are commonly 'sand-wedge casts' (primary infill) and 'ice-wedge pseudomorphs' (secondary infill), respectively. Transitional forms showing evidence of both types of infill are named 'composite-wedge casts'. The relative proportions of sediment and ice in the composite wedges are variable from one structure to another (French 2007). Kolstrup (1987) demonstrated that these three types of frost-fissure wedges can coexist in the same region depending upon the local characteristics. During thaw modification, the amount of ice in the initial structure determines the relative resemblance of the relic form. Sand-wedge casts, which are initially poor in ice, show vertical laminations, apophyses, bundles of sand veins, etc., and well-preserved, upturned strata (Harry & Gozdzik 1988; Murton & French 1993; Murton *et al.* 2000). Con-

versely, ice-wedge pseudomorphs show substantial thaw modifications compared with the original ice wedges; material from above and/or the sides of the wedge replaces the space left by the melting of the ice (secondary infill). These transformations can also be visible in the host sediment, which often exhibits *en echelon* microfaults and downturned strata (Harry & Gozdzik 1988; Murton & French 1993; Murton *et al.* 2000). In addition to these transformations related to the sagging of the host material, modifications can also be produced by fluvio-thermal erosion when water runs into the cavities left by the melting ice (Fortier *et al.* 2007; Godin *et al.* 2014).

The structures on the Magdalen Islands are interpreted as ice-wedge pseudomorphs and composite-wedge casts. The ice-wedge pseudomorphs are located at the BD, PT and AC (only AC-1) sites. These structures reveal several characteristics demonstrating that they were first filled by ice and were then distorted by melting (Table 5). The pseudomorph infillings are composed of material from the overlying and/or adjacent units, typical of the melting of former ice wedges (Harry & Gozdzik 1988; Murton & French 1993; French 2007). This is obvious in the AC-1 and at the BD sites where the subtidal unit (U2) clearly collapsed into wedges during ice melting (Figs 3, 4). AC-1 also contains a mix of grey sand and organic matter derived from the palaeosol located above; this organic material must therefore pre-date the infilling process. This is also evident at the PT site where coastal pebbles (U2) filled the wedges that cracked in altered sandstone (Figs 5, 6). The gradual infilling of the wedges caused the downwards deformation of the host strata. The infiltration of the often vertically realigned pebbles and the presence of sedimentary materials from the host sediment in the wedges suggest that they were deposited gradually as the ice melted (Harry & Gozdzik 1988; Mackay & Burn 2002). On either side of the structures, host material strata are deformed downwards and ruptured by several microfaults and well-developed *en echelon* downthrows (Harry & Gozdzik 1988; French 2007; Ewertowski 2009). These deformations occurred as a result of gravity during the melting of the ice wedge. Moreover, some structures show fluvio-thermal erosion (runoff and piping). The infill of the AC-1 pseudomorph is truncated by an unconformity that seems to be the bottom part of a gully. This unconformity is overlain by sediment that appears to come from the host sediment (sagging of the sides of the gully; Fig. 4A). The lower part of BD-2 was probably also widened by fluvio-thermal erosion when meltwater flowed into the fissure (Fig. 3B). Pseudomorphs often display enlargements (tunnels) at different depths (Fortier *et al.* 2007; French 2007). Finally, PT-1 is also characterized by a sudden enlargement in the upper part, probably formed by a stream channelled through the fissure (Fig. 5A, B). The light brown fine sands that fill the fissure and the channel (upper part) were presumably brought by runoff.

The other structures observed at the AC (AC-2 and AC-3) and GC sites do not exhibit such well-defined characteristics typical of ice-wedge pseudomorphs. Although these structures are filled mostly by material coming from the overlying palaeosol, the upturned strata of the host sediment was very well preserved, suggesting that the sagging related to thaw was minimal (e.g. Figs 4B–D, 6). In addition, the V-shape of the AC-2 structure is well preserved and also displays vertical laminations in its infill (Fig. 4B). This structure does not seem to have been modified by the melting of permafrost. Conversely, the bowl-shape of the AC-3 structure and its mixed infilling suggest some thaw modifications even though the upturned strata are very well preserved (Fig. 4D). The GC site structures are unusual; they were formed mostly in the sandstone bedrock and gravel and pebbles, and so it is not surprising that the host material was less susceptible to deformation during melting (thaw-stable). The infill is composed of coarse sediment from U2, becoming finer-grained from top to bottom, and the vertically aligned pebbles suggest a progressive infilling in narrow cavities with a 'sieving' of the sediment by these cavities. All these structures with absent or minimal thaw modifications were probably filled by a mixture of ice and mineral grains rather than pure ice. They are all interpreted as composite-wedge casts (French 2007).

Palaeoclimatic significance of the frost-fissure wedges on the Magdalen Islands

Frost-fissure wedges argue for perennial cold climate conditions that allowed recurrent frost-cracking in the ground. Temperature thresholds used for palaeoclimatic reconstructions were determined in modern periglacial environments. Since the 1960s (e.g. Lachenbruch 1962; Péwé 1962, 1966), it has generally been accepted that ice wedges form in coarse-grained sediment when the mean annual air temperature (MAAT) is lower than −6 to −8°C (Fortier & Allard 2005). Current MAAT on the Magdalen Islands is around 5°C (Bernatchez *et al.* 2008). Thus, from the temperature thresholds used in the literature, ice-wedge formation would require a ~12°C cooling relative to present. The combined depth of the ice-wedge pseudomorphs and composite-wedge casts and cryoturbations suggest a palaeo-active layer thickness of ≤1 m.

Implications of the new ^{14}C and OSL ages for the timing of the frost-fissure wedges

The radiocarbon and OSL dating results indicate that periglacial conditions and the development of

permafrost on the Magdalen Islands occurred after the last deglaciation. All the pseudomorphs on the Magdalen Islands penetrate subtidal or coastal deposits and therefore formed after the marine regression. These new results confirm that the frost-fissure wedges on the Magdalen Islands did not form during MIS 2 as suggested earlier (Poirier 1970; Laverdière & Guimond 1974; Guilbault 1976; Dredge *et al.* 1992). Our results rather suggest that permafrost occurred after the LGM glaciation, and that the archipelago remained under permafrost conditions for a prolonged period after the LGM, probably until the Younger Dryas. The cryopediments and asymmetrical valleys formed during that period needed the presence of perennially frozen ground to block the infiltration of water that led to the runoff forming these slightly inclined morphologies (Laverdière & Guimond 1974; Paquet 1989). However, uplift continued and relative sea level dropped throughout this period while the islands were frozen; new unfrozen sediment was continually being raised above the tidal level, allowing it to freeze. This scenario further supports the genetic interpretation of the frost fissures and is analogous to the observations described by Mackay & Burn (2002) in which they drained a lake in a permafrost environment and found that thermal-contraction cracking of the newly exposed sediment occurred in the first winter after draining.

Palaeoenvironmental significance

According to Shaw *et al.* (2006), the central part of the Gulf of St. Lawrence (Laurentian Channel) was deglaciated by *c.* 17 cal. ka BP. Owing to its proximity to the Laurentian Channel, the Magdalen Islands are believed to have been ice-free since *c.* 16 cal. ka BP (Josenhans 2007; Stea *et al.* 2011). After the deglaciation, the subtidal unit deposited around 12–11 ka ago at an elevation of ~20 m at the AC and BD sites indicates that at least the southern part of the Magdalen archipelago was submerged. Ice-wedge pseudomorph or composite-wedge cast infills that cross-cut this subtidal unit contain a combination of grey sand and organic matter that derived from the Ae and Ah podzol horizons, respectively. These horizons are observable throughout the archipelago. A warm period must have followed deglaciation to allow the establishment of vegetation and this palaeosol. As all the radiocarbon ages are derived from material that fell into the cavities left by the melting wedges, they are not contemporaneous with the periglacial activity that formed the wedges but provide a maximum age for the start of the degradation phase. OSL samples obtained on the AC site for the material that filled the cavities were dated to 10.7±0.7 and 9.8±0.7 ka; these are systematically younger than the organic matter (dated to between 13.1±0.2 and 12.4±0.2 cal. ka BP; Tables 4, 5). This systematic age difference may reflect the mean residence time of organic matter in soils (Walker 2005; Brovkin *et al.* 2008), or simply that organic production decreased significantly during the periglacial interval, so that only old carbon was available to be incorporated in the infill.

This sequence of a warmer climate during deglaciation followed by colder conditions is supported by Dredge *et al.* (1992), whose work suggested an abrupt climatic deterioration between 13.2 to 11.4 cal. ka BP owing to the reversion of shrub-tundra to herbaceous-tundra on the Magdalen Islands. A similar fluctuation was described in an extensive number of palaeoecological studies (see below) that detailed the postglacial climatic oscillations throughout the Maritime Provinces of southeastern Canada. The warmer conditions that followed the deglaciation, commonly associated with the Allerød warming event that occurred after 14 cal. ka BP, allowed the establishment of vegetation typical of boreal forest or shrub-tundra and active aquatic environments in New Brunswick and Nova Scotia (Mott *et al.* 1986, 2009; Mayle & Cwynar 1995a; Walker *et al.* 1996; Spooner *et al.* 2005). Other archives recorded a subsequent major cold event associated with the Younger Dryas from 12.7 to 11.4 cal. ka BP (e.g. Mott *et al.* 1986, 2009; Stea & Mott 1989, 1998, 2005; Levesque *et al.* 1993a, b; Cwynar & Levesque 1995; Mayle & Cwynar 1995a, b; Cwynar & Spear 2001; Spooner *et al.* 2005; Whitney *et al.* 2005). Moreover, ice-wedge pseudomorphs dated between 14–12.8 and 12.2 cal. ka BP were described by Liverman *et al.* (2000) in Newfoundland, and inactive rock glaciers described as geomorphic indicators of past permafrost (Humlum 1998) were associated with the Younger Dryas in Maine (USA; Putnam & Putnam 2009) and the Gaspésie peninsula (Québec; Hétu & Gray 2000; Hétu *et al.* 2003).

In summary, many palaeoecological and geomorphic studies demonstrate that after the LGM deglaciation the Allerød warming trend was interrupted by the Younger Dryas cold event. The Magdalen Islands recorded this climatic fluctuation firstly by the development of a palaeosol, and subsequently by the formation and infilling of the ice wedges and composite wedges described in this study.

Conclusions

Periglacial structures identified on the Magdalen Islands are interpreted as ice-wedge pseudomorphs and composite-wedge casts. Absolute ages for these structures were obtained for the first time and combined with detailed stratigraphical descriptions. The results from this combined approach indicate that the ice and composite wedges formed during a marine regression (between 12 and 11 cal. ka BP) after the formation of a well-developed podzol. We suggest that this cold period corresponds to the Younger Dryas.

The absolute chronological data presented in this paper refute the earlier interpretation that these periglacial features were formed much earlier during MIS 2. Our data support the interpretation that the periglacial structures of the Magdalen Islands described here formed after the last deglaciation.

Acknowledgements. – David Didier, Jean-Philippe Marchand, Benoit Vigneault and Gabriel Ladouceur are thanked for their valuable help in the field. The authors wish to acknowledge the support of the technical staff of the Nordic Laboratory for Luminescence Dating (NLL). The Natural Sciences and Engineering Research Council of Canada (NSERC), Fonds de recherche du Québec (FQRNT), the Coastal Geoscience Chair and the Canada Research Chair in Marine Geology provided financial support during the project. We also thank Jacob Wallinga and Hugh M. French for the constructive and helpful comments that greatly improved the manuscript. Comments by the Editor Jan A. Piotrowski are also much appreciated.

References

Alcock, F. J. 1941: The Magdalen Islands, their geology and mineral deposits. *Transactions of the Canadian Institute of Mine of Metallurgy 44*, 623–649.

Bernatchez, P., Fraser, C., Friesinger, S., Jolivet, Y., Dugas, S., Drejza, S. & Morissette, A. 2008: *Sensibilité des côtes et vulnérabilité des communautés du golfe du Saint-Laurent aux impacts des changements climatiques.* 256 pp. Laboratoire de dynamique et de gestion intégrée des zones côtières, Université du Québec à Rimouski, Rimouski.

Berra, F. & Felletti, F. 2011: Syndepositional tectonics recorded by soft-sediment deformation and liquefaction structures (continental Lower Permian sediments, Southern Alps, Northern Italy): stratigraphic significance. *Sedimentary Geology 235*, 249–263.

Bertran, P., Andrieux, E., Antoine, P., Coutard, S., Deschodt, L., Gardère, P., Hernandez, M., Legentil, C., Lenoble, A., Liard, M., Mercier, N., Moine, O., Sitzia, L. & Van Vliet-Lanoë, B. 2014: Distribution and chronology of Pleistocene permafrost features in France: database and first results. *Boreas 43*, 699–711.

Black, R. F. 1976: Periglacial features indicative of permafrost: Ice and soil wedges. *Quaternary Research 6*, 3–26.

Blott, S. J. & Pye, K. 2001: Gradistat: a grain size distribution and statistics package for the analysis of unconsolidated sediments. *Earth Surface Processes and Landforms 26*, 1237–1248.

Brandes, C. & Winsemann, J. 2013: Soft-sediment deformation structures in NW Germany caused by Late Pleistocene seismicity. *International Journal of Earth Sciences 102*, 2255–2274.

Brisebois, D. 1981: *Lithostratigraphie des strates Permo-Carbonifères de l'archipel des Îles de la Madeleine.* 48 pp. Ministère de l'Énergie et des Ressources du Québec, DPV-796, Québec.

Brovkin, V., Cherkinsky, A. & Goryachkin, S. 2008: Estimating soil carbon turnover using radiocarbon data: a case-study for European Russia. *Ecological Modelling 216*, 178–187.

Buylaert, J. P., Ghysels, G., Murray, A. S., Thomsen, K. J., Vandenberghe, D., De Corte, F., Heyse, I. & Van Den Haute, P. 2009: Optical dating of relict sand wedges and composite-wedge pseudomorphs in Flanders, Belgium. *Boreas 38*, 160–175.

Chalmers, R. 1895: Report on the surface geology of southern New Brunswick, north-western Nova Scotia and a portion of Prince Edward Island. *Geological Survey of Canada, Annual Report*, 144 pp.

Cheel, R. J. & Rust, B. R. 1986: A sequence of soft sediment deformation (dewatering) structures in Late Quaternary Subaqueous outwash near Ottawa, Canada. *Sedimentary Geology 47*, 77–93.

Clarke, J. M. 1911: Observations on the Magdalen Islands. *New York State Museum Bulletin 149*, 134–156.

Coleman, A. P. 1919: The glacial history of Prince Edward Island and the Magdalen Islands. *Proceedings and Transactions of the Royal Society of Canada 13*, 33–37.

Cunningham, A. C. & Wallinga, J. 2010: Selection of integration time intervals for quartz OSL decay curves. *Quaternary Geochronology 5*, 657–666.

Cwynar, L. C. & Levesque, A. J. 1995: Chironomid evidence for lateglacial climatic reversals in Maine. *Quaternary Research 43*, 405–413.

Cwynar, L. C. & Spear, R. W. 2001: Lateglacial climate change in the White Mountains of New Hampshire. *Quaternary Science Reviews 20*, 1265–1274.

Dionne, J.-C. & Laliberté, S. 2005: Horizontal cylindrical structures in an unconsolidated Quaternary deposit at Saint-Joachim, near Québec City (Canada). *Géographie physique et Quaternaire 59*, 75–80.

Dionne, J.-C. & Pérez Alberti, A. 2000: Structures cylindriques verticales dans un dépôt meuble Quaternaire, en Galice (Espagne). *Géographie physique et Quaternaire 54*, 343–349.

Dredge, L. A. & Grant, D. R. 1987: Glacial deformation of bedrock and sediment, Magdalen Islands and Nova Scotia, Canada: evidence for a regional grounded ice sheet. *In* der van Meer, J. J. M. (ed.): *Tills and Glaciotectonics: Proceedings of an INQUA Symposium on Genesis and Lithology of Glacial Deposits*, 183–195. Balkema, Rotterdam.

Dredge, L. A., Mott, R. J. & Grant, D. R. 1992: Quaternary stratigraphy, palaeoecology, and glacial geology, Iles de la Madeleine, Québec. *Canadian Journal of Earth Science 29*, 1981–1996.

Duller, G. A. T. 2003: Distinguishing quartz and feldspar in single grain luminescence measurements. *Radiation Measurements 37*, 161–165.

El Maarry, M. R., Kodikara, J., Wijessoriya, S., Markiewicz, W. J. & Thomas, N. 2012: Desiccation mechanism for formation of giant polygons on Earth and intermediate-sized polygons on Mars: results from a pre-fracture model. *Earth and Planetary Science Letters 323–324*, 19–26.

Ewertowski, M. 2009: Ice-wedge pseudomorphs and frost-cracking structures in Weichselian sediments, central-west Poland. *Permafrost and Periglacial Processes 20*, 316–330.

Fábián, S. Á., Kovács, J., Varga, G., Sipos, G., Horváth, Z., Thamó-Bozsó, E. & Tóth, G. 2014: Distribution of relict permafrost features in the Pannonian Basin, Hungary. *Boreas 43*, 722–732.

Folk, R. L. & Ward, W. C. 1957: Brazos River bar: a study in the significance of grain size parameters. *Journal of Sedimentary Petrology 27*, 3–26.

Fortier, D. & Allard, M. 2004: Late Holocene syngenetic ice-wedge polygons development, Bylot Island, Canadian Arctic Archipelago. *Canadian Journal of Earth Sciences 41*, 997–1012.

Fortier, D. & Allard, M. 2005: Frost-cracking Conditions, Bylot Island, Eastern Canadian Arctic Archipelago. *Permafrost and Periglacial Processes 16*, 145–161.

Fortier, D., Allard, M. & Shur, Y. 2007: Observation of rapid drainage system development by thermal erosion of ice wedges on Bylot Island, Canadian Arctic Archipelago. *Permafrost and Periglacial Processes 18*, 229–243.

French, H. M. 2007: *The Periglacial Environment*. 341 pp. Longman, New York.

French, H. M. 2008: Recent contributions to the study of past permafrost. *Permafrost and Periglacial Processes 19*, 179–194.

French, H. M., Demitroff, M. & Forman, S. L. 2003: Evidence for late-Pleistocene permafrost in the New Jersey Pine Barrens (Latitude 39N), Eastern USA. *Permafrost and Periglacial Processes 14*, 259–274.

French, H. M., Demitroff, M., Forman, S. L. & Newell, W. L. 2007: A chronology of late-Pleistocene permafrost events in southern New Jersey, Eastern USA. *Permafrost and Periglacial Processes 18*, 49–59.

Gangloff, P. 1974: Les structures cylindriques et l'évolution géomorphologiques d'une plage tardiglaciaire à Saint-Jérôme, Québec. *Revue de Géographie de Montréal 28*, 357–373.

Giles, P. S. 2008: Windsor Group (Late Mississippian) stratigraphy, Magadalen Islands, Quebec: a rare eastern Canadian record of late Visean basaltic volcanism. *Atlantic Geology 144*, 167–185.

Godin, E., Fortier, D. & Coulombe, S. 2014: Effects of thermo-erosion gullying on hydrologic flow networks, discharge and soil loss.

Environmental Research Letters 9, 1050, doi: 10.1088/1748-9326/9/10/105010.

Goldthwait, J. W. 1915: The occurrence of glacial drift on the Magdalen Islands. *Canada Geological Survey, Department of Mines, Museum Bulletin 14, Geological Series 25*, 11 pp.

Guérin, G., Mercier, N. & Adamiec, G. 2011: Dose-rate conversion factors: update. *Ancient TL 29*, 5–8.

Guilbault, N. 1976: Podzols et fentes de cryoturbation aux Îles-de-la-Madeleine. *Annales de l'Association canadienne-française pour l'avancement des sciences (ACFAS)*, 106 pp.

Hamelin, L. E. 1959: *Sables et mer aux Îles de la Madeleine*. 75 pp. Ministère de l'Industrie et du Commerce, Québec.

Hansen, V., Murray, A. S., Buylaert, J.-P., Yeo, E. Y. & Thomsen, K. J. 2015: A new irradiated quartz for beta source calibration. *Radiation Measurements*, http://dx.doi.org/10.1016/j.radmeas.2015.02.017.

Harry, D. G. & Gozdzik, J. S. 1988: Ice-wedges: growth, thaw transformation, and palaeoenvironmental significance. *Journal of Quaternary Science 3*, 39–55.

Hétu, B. & Gray, J. T. 2000: Effects of environmental change on scree slope development throughout the postglacial period in the Chic-Choc Mountains in the northern Gaspé Peninsula, Québec. *Geomorphology 32*, 335–355.

Hétu, B., Gray, J. T., Gangloff, P. & Archambault, B. 2003: Postglacial talus-derived rock glaciers in the Gaspé Peninsula, Québec (Canada). *In* Phillips, S. M., Springman, S. M. & Arenson, L. U. (eds.): *Proceedings of the 8th International Conference on Permafrost*, 389–394. Swetts & Zeitlinger, Lisse.

Huijzer, A. S. & Isarin, R. F. B. 1997: Reconstruction of past climates using multi-proxy evidence: an example of the Weishselian pleniglacial in northwest and central Europe. *Quaternary Science Reviews 16*, 513–533.

Humlum, O. 1998: The climatic significance of rock glaciers. *Permafrost and Periglacial Processes 9*, 375–395.

Johnson, S. Y. 1986: Water-escape structures in coarse-grained volcaniclastic, fluvial deposits of the Ellensburg Formation, south-central Washington. *Journal of Sedimentary Petrology 56*, 905–910.

Josenhans, H. 2007: Atlas of the marine environment and seabed geology of the Gulf of St. Lawrence. *Geological Survey of Canada, File 5346*, 142 pp.

Josenhans, H. & Lehman, S. 1999: Late glacial stratigraphy and history of the Gulf of St. Lawrence, Canada. *Canadian Journal of Earth Sciences 36*, 1327–1345.

Kolstrup, E. 1987: Frost-wedge casts in western Jutland and their possible implications for European periglacial research. *Zeitschrift für Geomorphologie 31*, 441–461.

Kovács, J., Fábián, S. A., Schweitzer, F. & Varga, G. 2007: A relict sand-wedge polygon site in North-central Hungary. *Permafrost and Periglacial Processes 18*, 379–384.

Lachenbruch, A. H. 1962: Mechanics of thermal contraction cracks and ice-wedge polygons in permafrost. *Geological Society of America, Special Paper 70*, 60 pp.

Laverdière, C. & Guimond, P. 1974: Un froid à sol fendre. *Geos 2*, 18–20.

Levesque, A. J., Mayle, F. E., Walker, I. R. & Cwynar, L. C. 1993a: A previously unrecognized late-glacial cold event in eastern North America. *Nature 361*, 623–626.

Levesque, A. J., Mayle, F. E., Walker, I. R. & Cwynar, L. C. 1993b: The amphi-Atlantic oscillation – a proposed late-glacial climatic event. *Quaternary Science Reviews 12*, 629–643.

Li, J. H. & Zhang, L. M. 2011: Study of desiccation crack initiation and development at ground surface. *Engineering Geology 123*, 347–358.

Liu, X. J. & Lai, Z. P. 2013: Optical dating of sand wedges and ice-wedge casts from Qinghai Lake area on the northeastern Qinghai-Tibetan Plateau and its palaeoenvironmental implications. *Boreas 42*, 333–341.

Liverman, D., Catto, N., Batterson, M., Mackenzie, C., Munro-Stasiuk, M., Scott, S. & Sommerville, A. 2000: Evidence of late glacial permafrost in Newfoundland. *Quaternary International 68*, 163–174.

Mackay, J. R. & Burn, C. R. 2002: The first 20 years (1978–1979 to 1998–1999) of active-layer development, Illisarvik experimental drained lake site, western Arctic coast, Canada. *Canadian Journal of Earth Sciences 39*, 1657–1674.

Mayle, F. E. & Cwynar, L. C. 1995a: A review of multi-proxy data for the Younger Dryas in Atlantic, Canada. *Quaternary Science Reviews 14*, 813–821.

Mayle, F. E. & Cwynar, L. C. 1995b: Impact of the Younger Dryas cooling event upon lowland vegetation of Maritime Canada. *Ecological Monographs 65*, 129–154.

Mordovskii, S. D., Vychuzhin, T. A. & Petrov, E. E. 1993: Coeffi-cients of linear expansion of freezing soils. *Journal of Mining Sciences 29*, 39–42.

Mott, R. J., Grant, D. R., Stea, R. R. & Occhietti, S. 1986: Late-glacial climatic oscillation in Atlantic Canada equivalent to the Allerød/younger Dryas event. *Nature 323*, 247–250.

Mott, R. J., Walker, I. R., Palmer, S. L. & Lavoie, M. 2009: A late-glacial – Holocene palaeoecological record from Pye Lake on the eastern shore of Nova Scotia, Canada. *Canadian Journal of Earth Sciences 46*, 637–650.

Murray, A. S. & Wintle, A. G. 2000: Luminescence dating of quartz using an improved single-aliquot regenerative-dose protocol. *Radiation Measurements 32*, 57–73.

Murray, A. S. & Wintle, A. G. 2003: The single aliquot regenerative dose protocol: potential for improvements in reliability. *Radiation Measurement 37*, 377–381.

Murray, A. S., Marten, R., Johnston, A. & Martin, P. 1987: Analysis for naturally occurring radionuclides at environmental concentrations by gamma spectrometry. *Journal of Radioanalytical and Nuclear Chemistry 115*, 263–288.

Murton, J. B. & French, H. M. 1993: Thaw modification of frost-fissure wedges, Richards Island, Pleistocene Mackenzie Delta, western Arctic Canada. *Journal of Quaternary Science 8*, 185–196.

Murton, J. B., French, H. M. & Lamothe, M. 1997: Late Wisconsinan erosion and eolian deposition, Summer Island area, Pleistocene Mackenzie Delta, Northwest Territories: optical dating and implications for glacial chronology. *Canadian Journal of Earth Sciences 34*, 190–199.

Murton, J. B., Worsley, P. & Gozdzik, J. 2000: Sand veins and wedges in cold aeolian environments. *Quaternary Science Reviews 19*, 899–922.

Neal, J. T., Langer, A. M. & Kerr, P. F. 1968: Giant desiccation polygons of Great Basin Playas. *Geological Society of America Bulletin 79*, 69–90.

Ogino, Y. & Matsuoka, N. 2007: Involutions resulting from annual freeze–thaw cycles: a laboratory simulation based on observations in Northeastern Japan. *Permafrost and Periglacial Processes 18*, 323–335.

Paquet, G. 1989: *L'évolution de la plate-forme gréseuse de l'Île du Cap-aux-Meules (Îles-de-la-Madeleine, Québec)*. 223 pp. Mémoire de maîtrise, Université de Montréal, Montréal.

Parent, P. & Dubois, J. M. M. 1988: Stratigraphie et événements du Quaternaire, Îles-de-la-Madeleine, Québec. – Indices de centres de dispersion glaciaire sur le plateau madeleinien. *In* Hétu, B. (ed.): Proceedings, 6e Congrès de l'Association québécoise pour l'étude du Quaternaire, 71. Rimouski, QC.

Péwé, T. L. 1962: Ice-wedges in permafrost. Lower Yukon river area near Galena, Alaska. *Biuletyn Peryglacjalny 11*, 65–76.

Péwé, T. L. 1966: Palaeoclimatic significance of fossil ice wedges. *Biuletyn Peryglacjalny 15*, 65–73.

Poirier, J. 1970: Fente de gel fossile aux Îles-de-la-Madeleine. *Revue de géographie de Montréal 24*, 319–320.

Prest, V. K., Terasme, J., Matthews, J. V. & Litchti-Federovich, S. 1976: Late-Quaternary Magdalen Islands, Quebec. *Maritime Sediments 12*, 39–59.

Putnam, A. E. & Putnam, D. E. 2009: Inactive and relict rock glaciers of the Deboullie Lakes Ecological Reserve, northern Maine, USA. *Journal of Quaternary Science 24*, 773–784.

Ravier, E., Buonchristiani, J.-F., Clerc, S., Guiraud, M., Menzies, J. & Portier, E. 2014: Sedimentological and deformational criteria for discriminating subglaciofluvial deposits from subaqueous ice-con-

tact fan deposits: a Pleistocene example (Ireland). *Sedimentology 61*, 1382–1410.

Reimer, P. J., Bard, E., Bayliss, A., Beck, J. W., Blackwell, P. G., Ramsey, C. B., Buck, C. E., Cheng, H., Edwards, R. L., Friedrich, M., Grootes, P. M., Guilderson, T. P., Haflidason, H., Hajdas, I., Hatté, C., Heaton, T. J., Hoffmann, D. L., Hogg, A. G., Hughen, K. A., Kaiser, K. F., Kromer, B., Manning, S. W., Niu, M., Reimer, R. W., Richards, D. A., Scott, E. M., Southon, J. R., Staff, R. A., Turney, C. S. M. & van der Plicht, J. 2013: INTCAL13 and MARINE13 radiocarbon age calibration curves 0–50,000 years cal BP. *Radiocarbon 55*, 1869–1887.

Rémillard, A. M., Hétu, B., Bernatchez, P. & Bertran, P. 2013: The Drift des Demoiselles on the southern Magdalen Islands (Quebec, Canada): sedimentological and micromorphological evidence of a glacial diamict of Late Wisconsinan. *Canadian Journal of Earth Sciences 50*, 545–563.

Richardson, J. 1881: Report of a geological exploration of the Magdalen Islands. *Geological Survey of Canada, Report of Progress, 1879–1880, part VIII*, 16 pp.

Shaw, J., Piper, D. J. W., Fader, G. B. J., King, E. L., Todd, B. J., Bell, T., Batterson, M. J. & Liverman, D. G. E. 2006: A conceptual model of the deglaciation of Atlantic Canada. *Quaternary Science Reviews 25*, 2059–2081.

Sooner, I. S., MacDonald, I., Beierle, B. & Timothy Jull, A. J. 2005: A multi-proxy lithostratigraphic record of Late Glacial and Holocene climate variability from Piper Lake, Nova Scotia. *Canadian Journal of Earth Sciences 42*, 2039–2049.

Stea, R. R. 2004: The Appalachian glacier complex in Maritime Canada. *In* Ehlers, J. & Gibbard, P. L. (eds.): *Quaternary Glaciations – Extent and Chronology, Part II: North America*, 213–232. Elsevier, New York.

Stea, R. R. & Mott, J. M. 1989: Deglaciation environments and evidence for glaciers of Younger Dryas age in Nova Scotia, Canada. *Boreas 18*, 169–187.

Stea, R. R. & Mott, J. M. 1998: Deglaciation of Nova Scotia: stratigraphy and chronology of lake sediment cores and buried organic sections. *Géographie physique et Quaternaire 52*, 3–21.

Stea, R. R. & Mott, J. M. 2005: Younger Dryas glacial advance in the southern Gulf of St. Lawrence, Canada: analogue for ice inception? *Boreas 34*, 345–362.

Stea, R. R., Piper, D. J. W., Fader, G. B. J. & Boyd, R. 1998: Wisconsinian glacial and sea-level history of Maritime Canada and the adjacent continental shelf: a correlation of land and sea events. *Geological Society of America Bulletin 110*, 821–845.

Stea, R. R., Seaman, A. A., Pronk, T., Parkhill, M. A., Allard, S. & Utting, D. 2011: The Appalachian Glacier Complex in Maritime Canada. *In* Ehlers, J. & Gibbard, P. L. (eds.): *Quaternary Glaciations – Extent and Chronology, Part II: North America*, 631–659. Elsevier, New York.

Su, D., Qiao, X., Sun, A., Li, H. & Somerville, I. A. 2014: Large earthquake-triggered liquefaction mounds and a carbonate sand volcano in the Mesoproterozoic Wumishan Formation, Beijing, North China. *Geological Journal 49*, 69–89.

Thomsen, K. J., Bøter-Jensen, L., Denby, P. M., Moska, P. & Murray, A. S. 2006: Developments in luminescence measurement techniques. *Radiation Measurements 41*, 768–773.

Van Huissteden, J., Vandenberghe, J. & Pollard, D. 2003: Palaeotemperatures reconstruction of the European permafrost zone during marine oxygen-isotope stage 3 compared with climate model results. *Journal of Quaternary Science 18*, 452–464.

Vandenberghe, J., Zhijiu, C., Liang, Z. & Wei, Z. 2004: Thermal-contraction crack network as evidence of Late-Pleistocene permafrost in Inner Mongolia, China. *Permafrost and Periglacial Processes 15*, 21–29.

Vaughan, J. M., England, J. H. & Evans, D. J. A. 2014: Glaciotectonic deformation and reinterpretation of the Worth Point stratigraphic sequence: Banks Island, NT, Canada. *Quaternary Science Reviews 91*, 124–145.

Walker, I. R., Levesque, A. J., Cwynar, L. C. & Lotter, A. F. 1996: An expanded surface-water palaeotemperature inference model for use with fossil midges from eastern Canada. *Journal of Paleolimnology 18*, 165–178.

Walker, M. 2005: *Quaternary Dating Methods*. 286 pp. John Wiley & Sons, Ltd., Chichester.

Whitney, B. S., Vincent, J. H. & Cwynar, L. C. 2005: A midge-based late-glacial temperature reconstruction from southwestern Nova Scotia. *Canadian Journal of Earth Sciences 42*, 2051–2057.

Wintle, A. G. & Murray, A. S. 2006: A review of quartz optically stimulated luminescence characteristics and their relevance in single-aliquot regeneration dating protocols. *Radiation Measurements 41*, 369–391.